



# Ohmic resistance affects microbial community and electrochemical kinetics in a multi-anode microbial electrochemical cell

Bipro Ranjan Dhar<sup>a</sup>, Hodon Ryu<sup>b</sup>, Jorge W. Santo Domingo<sup>b</sup>, Hyung-Sool Lee<sup>a,\*</sup>

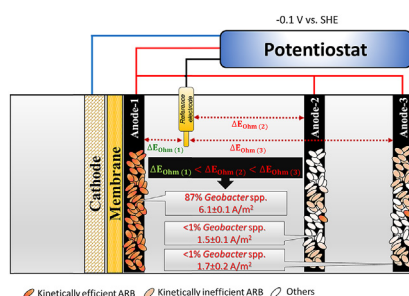
<sup>a</sup> Department of Civil & Environmental Engineering, University of Waterloo, 200 University Ave. West, ON N2L 3G1, Canada

<sup>b</sup> National Risk Management Research Laboratory, U.S. Environmental Protection Agency, 26 W. Martin Luther King Drive, Cincinnati, OH 45268, USA

## HIGHLIGHTS

- A multi-anode microbial electrochemical cell (MxC) was designed and operated.
- Microbial community and anode kinetics were evaluated for individual anodes.
- *Geobacter* species were dominant only on the anode closest to a reference electrode.
- Half-saturation anode potential was lower for the closest anode.
- High current density was produced only from the closest anode.

## GRAPHICAL ABSTRACT



## ARTICLE INFO

### Article history:

Received 3 June 2016

Received in revised form

23 August 2016

Accepted 12 September 2016

Available online 18 September 2016

### Keywords:

Anode potential

*Geobacter*

Half-saturation anode potential

Microbial electrochemical cells

Multi-anode

Ohmic energy loss

## ABSTRACT

Multi-anode microbial electrochemical cells (MxCs) are considered as one of the most promising configurations for scale-up of MxCs, but understanding of anode kinetics in multiple anodes is limited in the MxCs. In this study we assessed microbial community and electrochemical kinetic parameters for biofilms on individual anodes in a multi-anode MxC to better comprehend anode fundamentals. Microbial community analysis targeting 16S rRNA Illumina sequencing showed that *Geobacter* genus was abundant (87%) only on the biofilm anode closest to a reference electrode (low ohmic energy loss) in which current density was the highest among three anodes. In comparison, *Geobacter* populations were less than 1% for biofilms on other two anodes distant from the reference electrode (high ohmic energy loss), generating small current density. Half-saturation anode potential ( $E_{KA}$ ) was the lowest at  $-0.251$  to  $-0.242$  V (vs. standard hydrogen electrode) for the closest biofilm anode to the reference electrode, while  $E_{KA}$  was as high as  $-0.134$  V for the farthest anode. Our study proves that electric potential of individual anodes changed by ohmic energy loss shifts biofilm communities on individual anodes and consequently influences electron transfer kinetics on each anode in the multi-anode MxC.

© 2016 Elsevier B.V. All rights reserved.

## 1. Introduction

Our current society needs sustainable biotechnologies to build a

green cycle at the intersection of economy, environment, and energy. Microbial electrochemical cells (MxCs) that produce value-added chemicals from organic waste and wastewater can be one of the biotechnologies to catalyze establishment of the green circle [1–3]. MxCs should produce high current density (the fast yield of value-added products) with an acceptable range of exogenous energy to deploy MxCs in field. The kinetics on anodes primarily limits

\* Corresponding author.

E-mail address: [hyungsool@uwaterloo.ca](mailto:hyungsool@uwaterloo.ca) (H.-S. Lee).

current density in external energy dependent-MxCs, since electrode catalysts and exogenous energy accelerate abiotic reaction rates associated with ohmic and cathodic limitations [1–5]. While anodic reaction rate significantly depends on biological kinetic parameters, nanomaterials and new designs have been applied for anodes to improve the reaction rate [1,4–7]. The physical and chemical approaches on anodes increased current density by 10–25 A/m<sup>2</sup> [6,7], but they would not be readily applicable for large-scale MxCs, due to cost and scale-up issues [4,6,7]. Multi-anode configurations employing inexpensive electrodes could be a technically robust and economically viable option for scale up of MxCs [8–14], since multiple electrodes can improve mass transfer and biofilm formation per volume of anode chambers (or MxCs), propelling anode kinetics without footprint increase of MxCs [8,12–14]. However, literature has shown non-linear or sometimes trivial increase of current density in multi-anode MxCs over single-anode ones [9–12].

The small contribution of multiple anodes to the overall current density implies sluggish kinetics on the anodes, especially supplemental anodes. No studies, however, have assessed anode kinetics for individual anodes in multi-anode MxCs. Each anode would have heterogeneous conditions for electron transfer in biofilm anodes, such as mixing conditions, local substrate concentration, local pH, and ionic resistance between anodes, which could cause inconsistent, slow kinetics on individual anodes. Among these heterogeneities in multiple anodes, it is evident that multi-anode configuration creates ionic resistance between anodes different from single anode. Ohmic resistance (mainly ionic resistance) can change electric potential of individual anodes in multi-anode MxCs when electrode distance is far from each other. In this circumstance, anode potential of individual anodes would not be equivalent in multi-anode MxCs, which can change microbial community in biofilm anodes, leading to different biological and electrochemical electron transfer kinetics on each anode. The contribution of additional anodes to overall current density would be small when kinetically inferior ARB are enriched on supplemental anodes. Anode potential is a key parameter for enrichment of kinetically efficient anode-respiring bacteria (ARB) in biofilm anodes from mixed-culture inocula [14–16], although other factors (e.g., electrode materials and structures, substrate type and concentration, pH, and temperature) can affect ARB community in biofilm anodes [1–5,17–19]. For example, *Geobacter* genus, one of the most kinetically efficient ARB, became dominant in biofilm anodes and generated high current density (~10 A/m<sup>2</sup>) when mixed culture was inoculated at negative anode potential (−0.05 to −0.15 V vs. standard hydrogen electrode (SHE)) [14,15]. In comparison, more diverse ARB community was established at positive anode potential (+0.2 to +0.37 V vs. SHE), along with low current density (0.6–2 A/m<sup>2</sup>) in MxCs [14,16].

Improvement of current density using multiple anodes is based on the assumption that individual anodes generate comparable current density, thereby increasing the overall current density in multi-anode MxCs. If different microbial communities are built on individual anodes in multi-anode MxCs probably caused by ohmic energy loss among anodes, biological and electrochemical kinetics may not be conserved throughout multiple anodes. Then, current density generated from individual anodes is inconsistent, and multi-anode MxCs would not improve current density proportionally to the number of anodes. However, no studies have explored this important aspect yet.

This study was conducted to characterize microbial community and electrochemical kinetics in individual anodes for a multi-anode MxC. First, we quantified the current density in each anode of the MxC. Second, we identified dominant ARB in biofilm anodes by targeting 16S rRNA. Third, we characterized half-saturation anode

potential ( $E_{KA}$ ) for individual anodes to evaluate electrochemical kinetics. Finally, the implication of ohmic energy loss and its impacts on performance of multi-anode MxCs was summarized.

## 2. Methods

### 2.1. Configuration of multi-anode microbial electrochemical cell (MxC)

A dual chamber microbial electrochemical cell (MxC) equipped with three anode modules was fabricated using plexiglass (Fig. 1a) and the working volumes of an anode and a cathode chamber were 300 mL and 100 mL, respectively. A stainless steel mesh was employed for the cathode (Type 304, McMaster Carr, OH, USA) (Fig. 1b). High-density carbon fibers (2293-A, 24A Carbon Fiber, Fibre Glast Development Corp., Ohio, USA) that were connected with stainless steel current collectors were used as the anode module (Fig. 1c). Prior to use, the carbon fibers were pretreated for 3 days with nitric acid (1 mol/L), acetone (0.17 mol/L) and ethanol (0.17 mol/L) for 1 day in series, and then washed with MilliQ water (18.2 MΩ-cm). Three anode modules (anode-1, anode-2, and anode-3) were installed in the anode chamber of the MxC (Fig. 1a) and they were connected via copper wires. An anion exchange membrane (AMI-7001, Membranes International Inc., USA) was used as a separator between the anode and the cathode chamber, and the geometric surface area of the membrane was 28.1 cm<sup>2</sup>; current density was expressed per the membrane surface area in this study [20]. A reference electrode (Ag/AgCl reference electrode, MF-2052, Bioanalytical System Inc., USA) was placed between anode-1 and anode-2, and we reported electrode potential against standard hydrogen electrode (SHE) in this study. The distance between the reference electrode and anode-1 was 1.27 cm. The distances of the reference electrode from anode-2 and anode-3 were 3.81 cm and 6.35 cm, respectively (Fig. 1a).

### 2.2. Inoculation and operating conditions

We inoculated the MxC equipped with three anodes using 30 mL of anolyte from a mother MxC, which had been run with acetate medium [20] for over 1 year. The anode chamber was sparged with ultra-pure nitrogen (99.999%) for 20 min, and then the anode potential was set at −0.1 V vs. SHE using a potentiostat (BioLogic, VSP, Gamble Technologies, Canada). Current and applied voltage were recorded at every 120 s using EC-Lab for windows v 10.32 software in a personal computer connected with the potentiostat (BioLogic, VSP, Gamble Technologies, Canada). The MxC was operated in a temperature-controlled room at 25 °C. The anolyte was circulated using a peristaltic pump (Master Flex® L/S economy variable-speed drive, Cole-Parmer, Canada) at a flow rate of 25 mL/min for mixing. The cathode chamber was filled with tap water where hydrogen gas is produced, which allows us to focus on anodic reactions in the MxC [18]. The MxC was operated in batch mode for 3 days, and switched to continuous mode by feeding acetate medium (100 mM phosphate buffer) to the anode chamber at a flow rate of 15 mL/h with a peristaltic pump (Master Flex® L/S digital drive, Model 7523-80, Cole-Parmer, Canada); hydraulic residence time (HRT) in the anode chamber was kept at 20 h during the experiment. The average COD concentration of acetate medium was 2300 ± 40 mg COD/L.

At the constant anode potential and HRT, we started to run the MxC with three anode modules (anode-1, anode-2, and anode-3 for phase-1), then two modules (anode-1 and anode-2 for phase-2), and finally one module (anode-1 for phase-3). Anode modules were removed and reassembled in an anaerobic chamber (COY Type B Vinyl Anaerobic Chamber, COY Lab Products, USA) to avoid

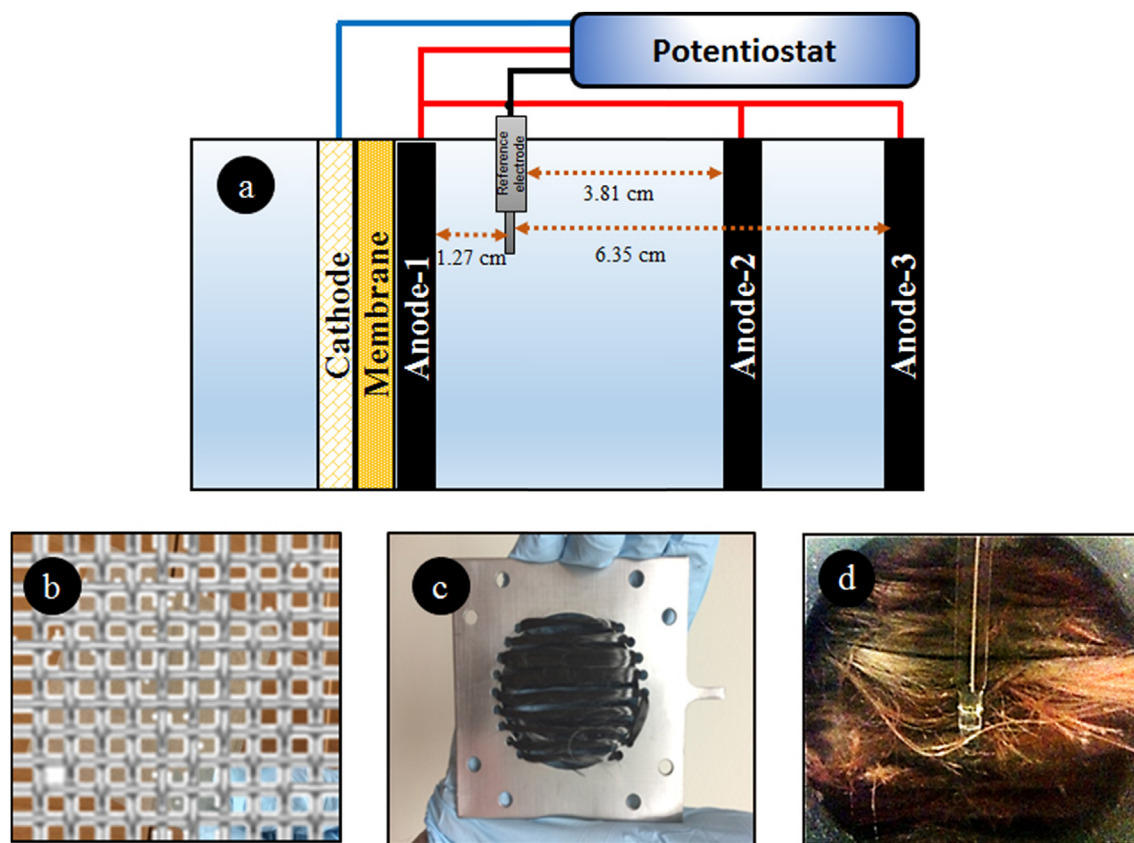


**Fig. 1.** (a) Schematic of multi-anode MxC configuration and experimental set-up, (b) cathode (stainless steel mesh), (c) anode module (carbon fibers integrated with a stainless steel current collector), (d) digital photograph of ARB biofilm grown on carbon-fiber anodes.

oxygen exposure to ARB. To evaluate the current density and estimate electrochemical kinetics for individual anode modules in phase-1 and phase-2, we temporally disconnected external connections between the anode modules and operated the MxC with each anode for 2.5 h. After that, we reconnected individual anodes with copper wires and operated as the multi-anode MxC.

### 2.3. Microbial community analysis

Total RNA were extracted from four anode biofilm samples as previously described with some minor modifications [21]. Briefly, the AllPrep DNA/RNA Mini Kit (Qiagen GmbH, Hilden, Germany) was used to extract total nucleic acid. RNA was further purified using Ambion TURBO DNA-free DNase kit (Life Technologies, Grand Island, NY). The concentration and purity of RNA were determined using Qubit RNA assay kits and the Qubit 2.0 Fluorometer (Life Technologies). We used barcoded 16S rRNA gene targeting primers (i.e., 515F and 806R) and sequenced the targeted product (i.e., 291 bp) in both directions using an Illumina MiSeq PE250 approach [22].

Sequence reads (16S rRNA-based) were processed and analyzed using Mothur software [23]. Sequence reads that did not fit the following criteria were discarded from further analyses: did not form contigs, deviated considerably from the expected PCR size product, identified as chimeras, had ambiguous bases, and had homopolymers greater than 7 bases long. Sequence reads were grouped at a 97% similarity and the consensus sequences were then identified using Mothur and the Silva database as a reference [24]. Excel was used to determine the overall relative abundance of representative sequences at different taxonomic levels (e.g., class, order, family, genus). Rare members (less than 10 sequences) were

excluded for the calculation of the relative abundance. Sequences were analyzed using Blast (<http://www.ncbi.nlm.nih.gov/BLAST>) and RDP classifier to further confirm their phylogenetic affiliation and to classify sequences at a low taxonomic level (genus and species) whenever possible [25].

### 2.4. Estimation of $E_{KA}$ and simulation of current density with the Nernst-Monod equation

The one-dimensional Nernst-Monod model was used to estimate half-saturation anode potential ( $E_{KA}$ ) for each anode module in three phases, which represents electrochemical kinetic features of ARB in biofilm anodes [18,26,27].  $E_{KA}$  was determined using forward low scanning cyclic voltammetry (LSCV) for individual anodes with three-electrode configuration (working, counter and reference electrodes). Anode potential was varied between  $-0.4$  and  $+0.4$  V vs. SHE at a scan rate of 1 mV/s using the potentiostat. The current and anode potential were recorded at every 5 s using EC-Lab for windows v 10.32 software in a personal computer connected with the potentiostat. To ensure the reproducibility of LSCV data, each CV test was conducted in triplicates, and the average data was reported. Since the potentiostat cannot compensated for ohmic energy loss between the anodes, the anode potential in the LSCV results were corrected using Eq. (1) to account for the ohmic energy loss between the anodes and reference electrode [27]:

$$\Delta E_{Ohm} = \frac{jL}{\kappa} \quad (1)$$

Where,  $\kappa$  is the conductivity of the anolyte (15.2 mS/cm),  $L$  is the

distance between anode and reference electrode (cm). The corrected anode potentials for ohmic energy loss were further used for the estimation of  $E_{KA}$  and Nernst-Monod model simulation. After determination of  $E_{KA}$ , the current density in response to corrected anode potential was simulated with the Nernst-Monod equation, described in Eq. (2). Acetate concentration was kept at 1250 to 1600 mg COD/L during the LSCV experiments to create acetate non-limiting conditions ( $S \gg K_s$ ), given that  $K_s$  for ARB is close to 119 mg COD/L [18].

$$j = j_{\max} \left[ \frac{1}{1 + \exp\left(-\frac{nF}{RT}(E_{\text{anode}} - E_{KA})\right)} \right] \quad (2)$$

where,  $j$  is the current density ( $A/m^2$ ),  $j_{\max}$  is the maximum current density ( $A/m^2$ ),  $K_s$  is the half-saturation substrate concentration (g COD/ $m^3$ ),  $S$  is the substrate (acetate) concentration in the bulk liquid (g COD/ $m^3$ ),  $R$  is the ideal gas constant (8.314 J/mol·K),  $F$  is the Faraday's constant (96,485 C/mol  $e^-$ ),  $T$  is the operating temperature of MxC (298.15 K),  $n$  is the number of electrons transferred,  $E_{\text{anode}}$  is the corrected anode potential (V), and  $E_{KA}$  is the half-saturation anode potential (V). For the simulation, it was assumed that  $n = 1$  [27].

## 2.5. Acetate quantification

Acetate concentration was measured using a gas chromatography (GC) (Model: Hewlett Packard HP 5890 Series II) equipped with a Nukol fused-silica capillary column and flame ionization detector (FID); Helium gas was used for the GC as a carrier gas [20].

## 3. Results and discussion

### 3.1. Current density from individual anodes

At steady state, the overall current density was the highest at  $9.15 \pm 0.36 A/m^2$  in the MxC equipped with three anode modules (phase-1). The current density from anode-1 (closest to the reference electrode) was high at  $\sim 6 A/m^2$ , which was consistently kept for three phases. In comparison, the current densities for anode-2 (electrode distance 3.81 cm from the reference electrode) and anode-3 (electrode distance 6.35 cm from the reference) were low at 1.4–1.7  $A/m^2$  in phase-1 and phase-2 (Fig. 2). This result clearly indicates that anode kinetics was not comparable in the three anodes: the fast kinetics for anode-1 and the sluggish kinetics for anode-2 and anode-3.

### 3.2. Estimation of anode potential corrected for ionic resistance in the multi-anode MxC

In this study, the potentials of three anodes electronically connected with copper wires were set at  $-0.1 V$  vs. SHE using the potentiostat, but the potentiostat does not have compensation function for ohmic energy loss between anodes. Instead, the potentiostat polarizes a counter electrode (here the cathode) to compensate for energy losses, such as the ohmic energy loss between an anode and a cathode, and electrode overpotential. This limited function of the potentiostat indicates that set anode potential (reading values of anode potential) can be different from intrinsic anode potential, when the ionic resistance between anodes and the reference electrode is significant [27–29]. Hence, the electric potential of individual anodes should be corrected for the ohmic energy loss between three anodes (mainly ionic resistance) for the MxC. Anode potentials corrected for ionic resistance using

Eq. (1) were summarized in Table 1, which clearly presents anode potentials deviated from the set value of  $-0.1 V$ . These potential deviations became significant at phase-1 (three anodes), due to higher current density. For instance, the electric potential of anode-3 corrected for ionic resistance was  $+0.3 V$  (0.4 V energy loss) at 9.15  $A/m^2$  (phase-1). In comparison, the corrected electric potential of anode-1 was close to the set value of  $-0.1 V$  ( $-0.04$  to  $-0.01 V$ ), due to closer electrode distance and consequently less energy loss. These results indicate that intrinsic electric potential of individual anodes in the multi-anode MxC was actually different from the set potential of  $-0.1 V$  because of ionic resistance. Anode potential polarized by ionic resistance (more positive anode potential) can diversify bacterial community in biofilm anodes, which can lower current density in MxCs [14–16]. We found high current density for anode-1 and low current density for the other two anodes (see Fig. 2). Estimation of intrinsic anode potential and trend of current density suggest that more diverse bacterial community might be built on anode-2 and anode-3 over anode-1, which possibly cause sluggish anode kinetics on anode-2 and anode-3.

### 3.3. Bacterial community on individual anodes

Fig. 3 shows community structures of bacteria in biofilms on individual anodes identified with a total of 147,468 rRNA sequences; the detailed result for microbial community analysis is provided in Supplementary material (See Table S1). The relative abundance of *Geobacter* spp., one of the most kinetically efficient ARB, was as high as 87% for biofilms on anode-1, which substantially decreased to  $<1\%$  for biofilms on the other two anodes. Family of *Rhodocyclaceae* became rich at 72% in anode-2, as the population of *Geobacter* spp. decreased. Anode-3 showed the most diverse community structure: Two genera of *Agrobacterium* and *Aeromonas*, and two families of *Rhodocyclaceae* and *Pseudomonadaceae* became abundant in anode-3. These results support that anode potential changed by ohmic energy loss (IR drop;  $I = \text{current (A)}$ ,  $R = \text{anolyte resistance } (\Omega)$ ) substantially influenced the selection of bacterial community structures on the individual anodes. The trend of bacterial community in the biofilms to anode potential is also consistent to the literature [14,15], showing abundant *Geobacter* genus at anode-1 (intrinsic anode potential from  $-0.04$  to  $-0.01 V$ ) but diverse bacterial community at anode-2 and anode-3 (intrinsic anode potential from  $+0.1$  to  $+0.3 V$ ).

Other dominant bacteria identified in anode-2 and anode-3 would be involved in extracellular electron transfer (EET). Microbial genomes identified EET genes in *Rhodoferrax* spp. (*Rhodocyclaceae*), *Pseudomonas* spp. (*Pseudomonadaceae*), and *Aeromonas* spp. homologous to the iron-reducing EET pathway of *Shewanella oneidensis* MR-1 [30–33]. These microorganisms were relatively abundant for anode-2, and anode-3. The family of *Rhodocyclaceae* are also identified as dominant ARB in biofilm anodes of acetate-fed MxCs, but its EET mechanism is unclear [34–36]. *Aeromonas* spp. identified as one of the major ARB for anode-3 (19%) can use exogenous shuttling compound or conductive nanowires for EET [32,37–39]. *Agrobacterium* spp. identified for anode-3 (4.8%) was also found in anode biofilms fed with acetate [40–42]. *Agrobacterium* spp., well known for biofilm formation and production of extracellular polymeric substances, has putative nanowires [43,44]. The *Pseudomonadaceae* family (e.g., *Pseudomonas* spp.) has been found to produce conductive nanowires or endogenous shuttling compounds to facilitate EET in MxCs fed with acetate [45,46]. It seems that *Agrobacterium* spp., *Aeromonas* spp., and some genera from *Rhodocyclaceae* and *Pseudomonadaceae* families would be involved in EET in the MxC. However, lower current densities for anode-2, and anode-3 imply that their kinetic



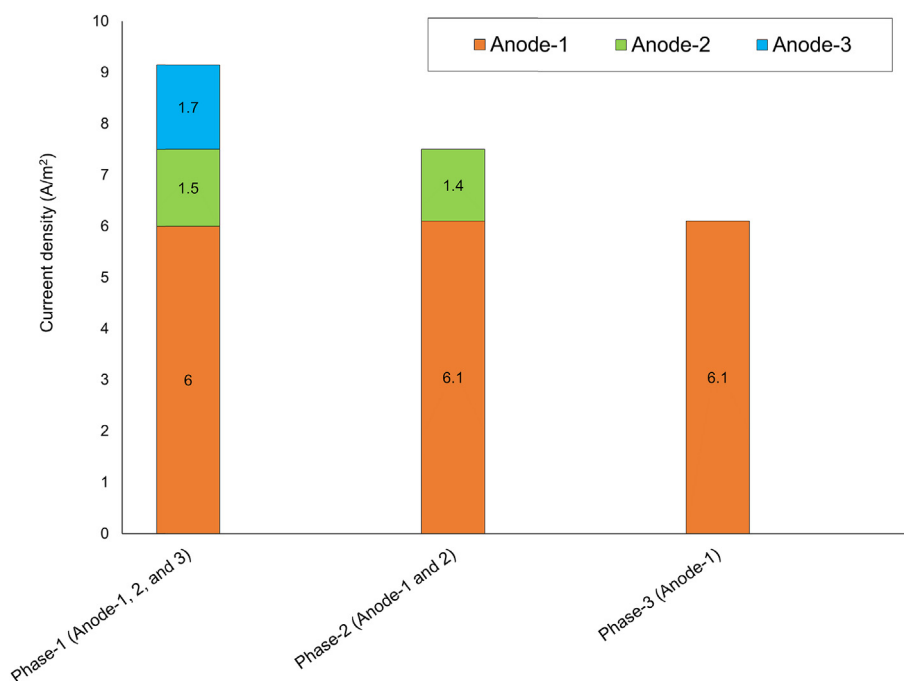


Fig. 2. Current density from individual anode modules at different experimental phases.

Table 1

Anode potentials corrected for ionic resistances.

Phase	Anode	Electrode distance from reference electrode (cm)	Corrected anode potential (V vs. SHE)	Current density (A/m <sup>2</sup> )
1	Anode-1	1.27	−0.01	9.15 ± 0.36
	Anode-2	3.81	+0.14	
	Anode-3	6.35	+0.30	
2	Anode-1	1.27	−0.03	7.5 ± 0.20
	Anode-2	3.81	+0.10	
3	Anode-1	1.27	−0.04	6.1 ± 0.1

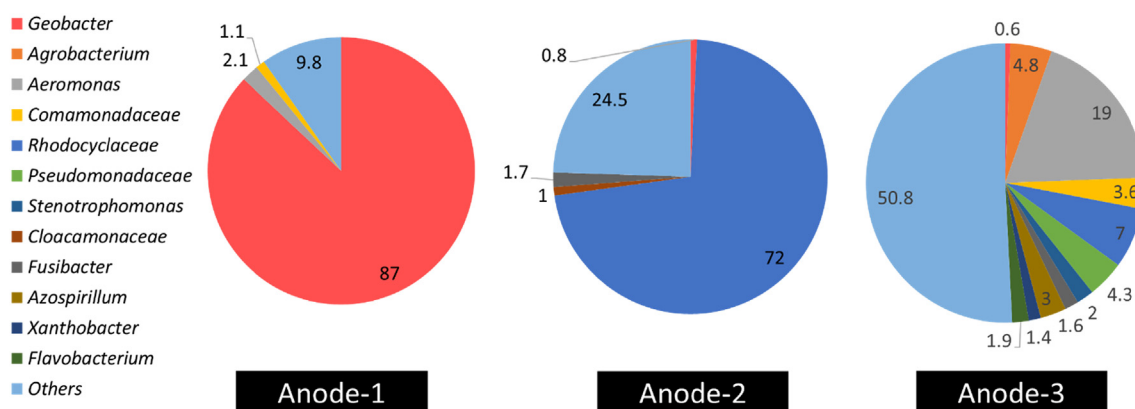
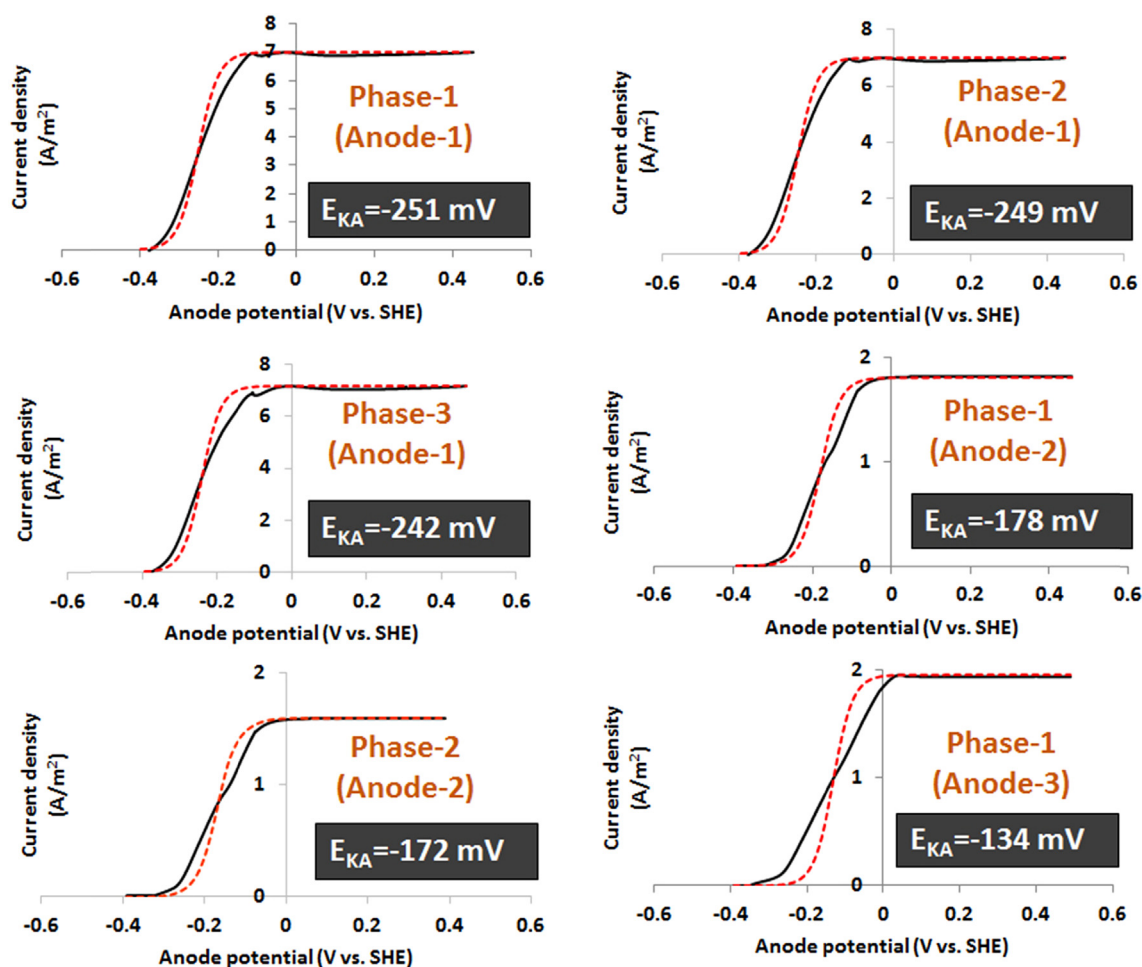


Fig. 3. Microbial community structures in biofilms on individual anodes.

features would be inferior to *Geobacter* genus. Multi anodes should be placed close to a reference electrode in microbial electrolysis cells or to a cathode in microbial fuel cells for minimizing ionic resistance among anodes and keeping anode potentials less than 0 V vs. SHE for enrichment of kinetically efficient ARB (e.g., *Geobacter* genus).

### 3.4. Estimation of half-saturation anode potential ( $E_{KA}$ ) for individual anode biofilms

Fig. 4 shows the forward scan LSCV patterns (the average of triplicate tests) for individual anode modules.  $E_{KA}$  tended to increase (more positive) as the maximum current density ( $j_{max}$ )



**Fig. 4.** Experimental and simulated current density profiles to anode potential. The black lines indicate experimental LSCVs at a scan rate of 1 mV/s for the steady-state MxC. The dotted red line indicates simulations with estimated  $E_{KA}$  and the Nernst-Monod equation. (For interpretation of the references to colour in this figure legend, the reader is referred to the web version of this article.)

decreased: high  $E_{KA}$  with low  $j_{max}$ .  $E_{KA}$  ranged from  $-0.251 \pm 0.001$  to  $-0.242 \pm 0$  V (vs. SHE) for anode-1 ( $j_{max} 7.1 \pm 0.15$  A/m<sup>2</sup>), which was as high as  $-0.134 \pm 0.001$  V for anode-3 ( $j_{max} 1.88 \pm 0.07$  A/m<sup>2</sup>). Current density is earlier saturated for substrate concentration as  $E_{KA}$  becomes more negative, indicating high current density with small energy loss [18,26,27]. The highest catalytic function (the highest  $j_{max}$  and the lowest  $E_{KA}$ ) was found for the biofilms on anode-1 with the largest population of *Geobacter* genus. Low  $j_{max}$  and high  $E_{KA}$  were observed for anode-2 and anode-3, along with increase of *Agrobacterium* spp., *Aeromonas* spp., and *Rhodocyclaceae* and *Pseudomonadaceae* families. High  $E_{KA}$  for anode-2 and anode-3 implies inferior electrochemical kinetics for these four ARB candidates.  $E_{KA}$  values for anode-1 and anode-2 were consistent to phase 1 to phase 3, indicating that electrochemical kinetics of biofilm anodes was conserved during the experiment (see Fig. 4).

Estimated  $E_{KA}$  values were used to simulate current density against anode potential using the Nernst-Monod model (Eq. (2)) under substrate non-limiting conditions. As shown in Fig. 4, sigmoidal patterns of Nernst-Monod simulations well match experimental LSCVs for anode-1, implying that conduction-based EET would occur for this anode [18,26,27,47]. In comparison, the simulated polarization curves were deviated from experimental LSCVs for anode-2 and anode-3, suggesting EET mechanisms other than conduction or significant energy loss in conductive EET (e.g., poor biofilm conductivity) for anode-2 and anode-3 [18,26,27,47].

#### 4. Conclusions

Multi-anode configurations improved current density, but current density did not increase proportional to the number of anodes, mainly due to different bacteria communities established on individual anodes. Ohmic energy loss that depends on current density, electrolyte resistance and electrode distance changed intrinsic electric potential of each anode in the multi-anode MxC, which significantly shifted biofilm community among three anodes. *Geobacter* genus was only rich at anode-1 close to the reference electrode, while its population substantially decreased in biofilms on anode-2 and anode-3 distant from the reference electrode. In addition, relatively higher  $E_{KA}$  were observed for anode-2 and anode-3 than that for anode-1, implying inefficient electrochemical kinetics. Our study clearly shows that ionic resistances between multiple anodes can polarize anode potentials, leading to substantial change of key ARB players and sluggish anode kinetics.

#### Acknowledgements

We thank Michael Elk for technical assistance. We also thank Dr. Junyoung An and Dr. Elsayed Elbeshbishy for their comments on experimental plan and fabrication of a reactor. This work was financially supported by Natural Sciences and Engineering Research Council of Canada (STPGP 478972). The U.S.

Environmental Protection Agency, through its Office of Research and Development, partially funded this research. This work has been subjected to the agency's administrative review and has been approved for external publication. Any opinions expressed in this paper are those of the authors and do not necessarily reflect the views of the agency; therefore, no official endorsement should be inferred. Any mention of trade names or commercial products does not constitute endorsement or recommendation for use.

## Appendix A. Supplementary data

Supplementary data related to this article can be found at <http://dx.doi.org/10.1016/j.jpowsour.2016.09.055>.

## References

- [1] B.E. Logan, M.J. Wallack, K.Y. Kim, W. He, Y. Feng, P.E. Saikaly, *Environ. Sci. Technol. Lett.* 2 (8) (2015) 206–214.
- [2] A. Escapa, R. Mateos, E.J. Martínez, J. Blanes, *Renew. Sustain. Energy Rev.* 55 (2016) 942–956.
- [3] C.S. He, Z.X. Mu, H.Y. Yang, Y.Z. Wang, Y. Mu, H.Q. Yu, *Chemosphere* 140 (2015) 12–17.
- [4] M. Ghasemi, M. Ismail, S.K. Kamarudin, K. Saeedfar, W.R.W. Daud, S.H. Hassan, L.Y. Heng, J. Alam, S.E. Oh, *Appl. Energy* 102 (2013) 1050–1056.
- [5] C. Santoro, A. Serov, C.W. Narvaez Villarrubia, S. Stariha, S. Babanova, A.J. Schuler, K. Artyushkova, P. Atanassov, *ChemSusChem* 8 (5) (2015) 828–834.
- [6] X. Xie, M. Ye, L. Hu, N. Liu, J.R. McDonough, W. Chen, H.N. Alshareef, C.S. Criddle, Y. Cui, *Energy Environ. Sci.* 5 (1) (2012) 5265–5270.
- [7] Z. He, J. Liu, Y. Qiao, C.M. Li, T.T.Y. Tan, *Nano Lett.* 12 (9) (2012) 4738–4741.
- [8] Y. Ahn, B.E. Logan, *Appl. Microbiol. Biotechnol.* 93 (5) (2012) 2241–2248.
- [9] V. Lanas, B.E. Logan, *Bioresour. Technol.* 148 (2013) 379–385.
- [10] A.J. Hutchinson, J.C. Tokash, B.E. Logan, *J. Power Sources* 196 (22) (2011) 9213–9219.
- [11] D. Jiang, M. Curtis, E. Troop, K. Scheible, J. McGrath, B. Hu, S. Suib, D. Raymond, B. Li, *Int. J. Hydrogen Energy* 36 (1) (2011) 876–884.
- [12] D. Jiang, B. Li, *Biochem. Eng. J.* 47 (1) (2009) 31–37.
- [13] L. Ren, Y. Ahn, H. Hou, F. Zhang, B.E. Logan, *J. Power Sources* 257 (2014) 454–460.
- [14] C.I. Torres, R. Krajmalnik-Brown, P. Parameswaran, A.K. Marcus, G. Wanger, Y.A. Gorby, B.E. Rittmann, *Environ. Sci. Technol.* 43 (24) (2009) 9519–9524.
- [15] A.S. Commault, G. Lear, M.A. Packer, R.J. Weld, *Bioresour. Technol.* 139 (2013) 226–234.
- [16] A. Kumar, A. Siggins, K. Katuri, T. Mahony, V. O'Flaherty, P. Lens, D. Leech, *Chem. Eng. J.* 230 (2013) 532–536.
- [17] B.E. Logan, K. Rabaey, *Science* 337 (6095) (2012) 686–690.
- [18] H.S. Lee, C.I. Torres, B.E. Rittmann, *Environ. Sci. Technol.* 43 (19) (2009) 7571–7577.
- [19] C.I. Torres, A.K. Marcus, B.E. Rittmann, *Biotechnol. Bioeng.* 100 (5) (2008) 872–881.
- [20] B.R. Dhar, Y. Gao, H. Yeo, H.S. Lee, *Bioresour. Technol.* 148 (2013) 208–214.
- [21] T. Pitkanen, H. Ryu, M. Elk, A.M. Hokajärvi, S. Siponen, A. Vepsäläinen, P. Räsänen, J.W. Santo Domingo, *Environ. Sci. Technol.* 47 (23) (2013) 13611–13620.
- [22] J.G. Caporaso, C.L. Lauber, W.A. Walters, D. Berg-lyons, C.A. Lozupone, P.J. Turnbaugh, N. Fierer, R. Knight, *Proc. Natl. Acad. Sci. U.S.A.* 108 (Suppl. 1) (2011) 4516–4522.
- [23] P.D. Schloss, S.L. Westcott, T. Ryabin, J.R. Hall, M. Hartmann, E.B. Hollister, R.A. Lesniewski, B.B. Oakley, D.H. Parks, C.J. Robinson, J.W. Sahl, *Appl. Environ. Microbiol.* 75 (23) (2009) 7537–7541.
- [24] Q. Wang, G.M. Garrity, J.M. Tiedje, J.R. Cole, *Appl. Environ. Microbiol.* 73 (16) (2007) 5261–5267.
- [25] C. Quast, E. Pruesse, P. Yilmaz, J. Gerken, T. Schweer, P. Yarza, J. Peplies, F.O. Glöckner, *Nucleic Acids Res.* 41 (D1) (2013) D590–D596.
- [26] A.K. Marcus, C.I. Torres, B.E. Rittmann, *Biotechnol. Bioeng.* 98 (6) (2007) 1171–1182.
- [27] C.I. Torres, A.K. Marcus, P. Parameswaran, B.E. Rittmann, *Environ. Sci. Technol.* 42 (17) (2008) 6593–6597.
- [28] F. Zhang, J. Liu, I. Ivanov, M.C. Hatzell, W. Yang, Y. Ahn, B.E. Logan, *Biotechnol. Bioeng.* 111 (10) (2014) 1931–1939.
- [29] S.A. Patil, S. Gildemyn, D. Pant, K. Zengler, B.E. Logan, K. Rabaey, *Biotechnol. Adv.* 33 (6) (2015) 736–744.
- [30] K.T. Finneran, C.V. Johnsen, D.R. Lovley, *Int. J. Syst. Evol. Microbiol.* 53 (3) (2003) 669–673.
- [31] S.K. Chaudhuri, D.R. Lovley, *Nat. Biotechnol.* 21 (10) (2003) 1229–1232.
- [32] C.A. Pham, S.J. Jung, N.T. Phung, J. Lee, I.S. Chang, B.H. Kim, H. Yi, J.A. Chun, *FEMS Microbiol. Lett.* 223 (1) (2003) 129–134.
- [33] L. Shi, K.M. Rosso, T.A. Clarke, D.J. Richardson, J.M. Zachara, J.K. Fredrickson, *Front. Microbiol.* 3 (2012).
- [34] D. Xing, S. Cheng, B.E. Logan, J.M. Regan, *Appl. Microbiol. Biotechnol.* 85 (5) (2010) 1575–1587.
- [35] A. Kozuma, T. Kasai, G. Nakagawa, A. Yamamuro, T. Abe, K. Watanabe, *PLoS ONE* 8 (11) (2013) e77443.
- [36] Y. Song, L. Xiao, I. Jayamani, Z. He, A.M. Cupples, *J. Microbiol. Methods* 108 (2015) 4–11.
- [37] K. Chung, S. Okabe, *Biotechnol. Bioeng.* 104 (5) (2009) 901–910.
- [38] L. Castro, R. Zhang, J.A. Muñoz, F. González, M.L. Blázquez, W. Sand, A. Ballester, *Biofouling* 30 (4) (2014) 501–511.
- [39] L. Castro, M. Vera, M.J.A. Muñoz, M.L. Blázquez, F. González, W. Sand, A. Ballester, *Res. Microbiol.* 165 (9) (2014) 794–802.
- [40] M. Sun, Z.H. Tong, G.P. Sheng, Y.Z. Chen, F. Zhang, Z.X. Mu, H.L. Wang, R.J. Zeng, X.W. Liu, H.Q. Yu, L. Wei, *Biosens. Bioelectron.* 26 (2) (2010) 470–476.
- [41] W. Liu, A. Wang, D. Sun, N. Ren, Y. Zhang, J. Zhou, J. Biotechnol. 157 (4) (2012) 628–632.
- [42] H. Hossini, A. Rezaee, B. Ayati, A.H. Mahvi, *RSC Adv.* 5 (89) (2015) 72699–72708.
- [43] J.P. Kenney, J.B. Fein, *Chem. Geol.* 286 (3) (2011) 109–117.
- [44] J. Aguilar, J. Zupan, T.A. Cameron, P.C. Zambryski, *Proc. Natl. Acad. Sci. U.S.A.* 107 (8) (2010) 3758–3763.
- [45] N. Boon, P. Aelterman, P. Clauwaert, L. De Schampelaire, L. Vanhaecke, K. De Maeyer, M. Höfte, W. Verstraete, K. Rabaey, *Appl. Microbiol. Biotechnol.* 77 (5) (2008) 1119–1129.
- [46] N.S. Malvankar, M. Vargas, K.P. Nevin, A.E. Franks, C. Leang, B.C. Kim, K. Inoue, T. Mester, S.F. Covalla, J.P. Johnson, V.M. Rotello, *Nat. Nanotechnol.* 6 (9) (2011) 573–579.
- [47] R. Renslow, J. Babauta, A. Kuprat, J. Schenk, C. Ivory, J. Fredrickson, H. Beyenal, *Phys. Chem. Chem. Phys.* 15 (44) (2013) 19262–19283.